
Formulation of 3D finite elements for hepatic radiofrequency ablation

Yansheng Jiang and Stefaan Mulier

Department of Radiology, Gasthuisberg University Hospital,
Herestraat 49, 3000, Leuven, Belgium
E-mail: yanshengjiang@hotmail.com
E-mail: stefaan.mulier@skynet.be

Wang Chong

Departamento de Tecnologia,
Universidade Regional de Noroeste do Estado do Rio Grande do Sul,
Rua Prefeito Rudi Franke, 540 CP 121,
Panambi – RS, 98.280-000, Brazil
E-mail: wang@unijui.edu.br

Michele Cristiane Diel Rambo

Departamento de Física, Estatística, Matemática,
Universidade Regional de Noroeste do Estado do Rio Grande do Sul,
Rua do Comércio, 3000, Bairro Universitário,
Ijuí-RS, 98700-000, Brazil
E-mail: michelecdrambo@hotmail.com

Feng Chen, Guy Marchal and Yicheng Ni*

Department of Radiology, Gasthuisberg University Hospital,
Herestraat 49, 3000, Leuven, Belgium
E-mail: feng.chen@med.kuleuven.be
E-mail: guy.marchal@uz.kuleuven.be
E-mail: Yicheng.Ni@med.kuleuven.be

*Corresponding author

Abstract: Radiofrequency ablation (RFA) is being used as one of the minimally invasive treatments for unresectable primary and metastatic liver tumours. The variables identified to have significant impact on RF heating include electrical conductivity of the tumour and surrounding tissue, thermal conductivity of tissue, tissue perfusion and RF generator output. These constitute a dynamic and complex matter that makes it difficult to achieve an optimal RFA in clinical practice. This study was intended to propose a specialised three dimensional (3D) finite element modelling in order to develop a fast analysis tool for clinicians to optimise RFA parameters and to predict the ablation outcomes.

Keywords: hepatic tumour; radiofrequency ablation; RFA; finite element modelling; tetrahedral element; Joule heat.

Reference to this paper should be made as follows: Jiang, Y., Mulier, S., Chong, W., Diel Rambo, M.C., Chen, F., Marchal, G. and Ni, Y. (2010) 'Formulation of 3D finite elements for hepatic radiofrequency ablation', *Int. J. Modelling, Identification and Control*, Vol. 9, No. 3, pp.225–235.

Biographical notes: Yansheng Jiang graduated from Wuhan University of Technology, China in 1982. He received his PhD in Applied Sciences from State University of Liège, Belgium in 1987. He joined Polyflow company (now a part of ANSYS) in 1991 as a Software Engineer in developing finite element methods in non-Newtonian fluid mechanics. From 2005 to 2007, as Visiting Professor, he taught courses in Mechanical Engineering at Universidade Regional do Noroeste do Estado do Rio Grande do Sul, Brazil. He has been interested in developing various numerical methods in engineering such as boundary element methods, parallel computing and point collocation methods. His current research topic is finite element modelling of radiofrequency ablation of tumour.

Stefaan Mulier graduated as an MD in 1988 and became a General Surgeon in 1995. He followed special complementary trainings in abdominal surgery and surgical oncology at the University Hospital of the Catholic University of Leuven. Since 1997, he has been actively engaged in RFA research at KUL with numerous publications in leading journals of medical sciences.

Wang Chong is an Associate Professor of Mechanical Engineering at Universidade Regional do Noroeste do Estado do Rio Grande do Sul in Brazil. He graduated from the University of Science and Technology of China (USTC) in 1982, received an MSc from the Chinese Academy of Sciences (CAS) in 1985 and earned his Doctorate from China University of Mining and Technology (CUMT) in 1988. As a Lecturer, he taught graduate courses in CUMT from 1989 to 1992; as a Visiting Scientist, he worked at the Federal University of São Carlos from 1993 to 1995 and at the University of São Paulo in Brazil from 1996 to 1997.

Michele Cristiane Diel Rambo graduated in Mathematics in 2005 and obtained a Master's in Applied Mathematics in 2008 from Universidade Regional do Noroeste do Estado do Rio Grande do Sul, Brazil, with a dissertation entitled of Modelagem matemática da distribuição de temperatura na ablação por radiofrequência devido a um ponto com uma fonte de corrente elétrica. She works at the College of Education, Science and Literature of Paraiso, Brazil.

Feng Chen obtained a Bachelor's degree of Medicine in 1984 and a Master's of Radiology in 1987 from Nanjing Railway Medical College, P.R. China. He received his PhD in Medical Science from the University of Leuven in 2007. Now, he is working at the University of Leuven, Belgium. His main research areas include stroke imaging, imaging of tumour angiogenesis and MR contrast media.

Guy Marchal received his undergraduate medical education at the Catholic University of Louvain, Medical School and entitled his MD in 1970. Postgraduate training in Radiology was received at the University Hospitals in Leuven and concluded with the Board certification in Radiology in 1973. He obtained his PhD on a dissertation entitled, 'Contributions to tissue characterisation in US, CT and MRI'. He has been Full Professor since 1992 and Chairman of the Department of Radiology of the University hospitals of Leuven since 1997. He is the Research Director of the Laboratory for Medical Imaging (Radiology/ESAT), past-President of the Royal Belgian Society of Radiology and Member of numerous committees/boards at the University and in different scientific organisations. He is the author or co-author of approximately 650 papers on medical imaging.

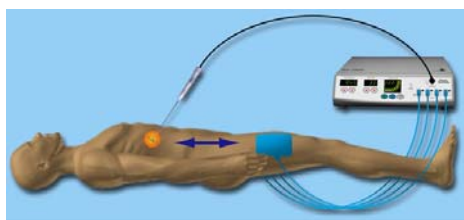
Yicheng Ni, with an MD background in China, was appointed with a permanent Professorship at Catholic University Leuven (KUL), Belgium in 1995 upon receiving his PhD and since then, he is the Director of the Radiology Laboratory in the Faculty of Medicine of the KUL. His academic interests have been focused on biomedical imaging, innovative therapy and contrast media research related to life-threatening diseases. He has discovered necrosis-avid contrast agents (NACAs) for visualisation of heart attack and assessment of minimally invasive cancer therapies; guided many Doctoral and Master students including the first PhD on cancer radiofrequency ablation (RFA), which has now been widely applied in clinical oncology; filed over a dozen of patent applications; published more than hundred quality journal papers and book chapters; developed a dual targeting anticancer theragnostic strategy and received numerous academic awards and honours.

1 Introduction

Primary and secondary hepatic cancers are among the most commonly encountered malignancies in clinic with annually over one million new cases throughout the world. Surgical resection is presently the first choice of treatment for resectable primary and metastatic liver tumours. However, it is not applicable in many patients due to multifocal disease, inadequate functional hepatic reserve, or comorbidity. Radiofrequency ablation (RFA) has emerged as a minimally invasive therapy for unresectable liver tumours by means of heating tumour cells above a lethal threshold (around 50°C). Typically, during a RFA session, an electrode is introduced into the tumour. An electrical alternating current (AC) flows

from the electrode through the tissues back to the ground pad. Both electrode and ground pad are connected to a generator (Figure 1). The tissue around the electrode is coagulated due to the heat produced by the electrical resistance. The frequency of current is in the range of medium wave ($20 \text{ kHz} < \text{RF} < 20 \text{ MHz}$), more specifically around 500 kHz. It is high enough to cause molecular frictional heat without stimulating neuromuscular reaction and electrolysis and low enough to confine energy transmission to a more controllable tissue mass without generating excessive radiation. AC stronger than 100 mA at a lower frequency of 50 Hz (household mains electricity) is known to cause fatal electrocution and ventricular fibrillation (Ni et al., 2005).

Figure 1 RFA in a monopolar mode (see online version for colours)



In practice, the positioning of the electrode tip in tumour is generally guided by an imaging modality such as ultrasound, computed tomography (CT) or magnetic resonance imaging (MRI). Because of respiratory movement of diaphragm, the change of liver position may be up to 3–5 cm. Hence, the positioning of the electrode tip often requires experience of the interventionalists.

To date, monitoring of the coagulation zone during the RFA procedure still remains a challenging issue under intense research. In case of ultrasound, the steam bubbles create a hyperechogenic cloud, obscuring the tumour and preventing correct monitoring; in case of CT, the soft tissue contrast is insufficient to distinguish viable and dead tissues; while in case of MRI, the interference between radiofrequency current and magnetic field makes the monitoring difficult or impossible. For these reasons, usually the clinical results cannot be properly evaluated during the RFA procedure, but only afterwards. After RFA, the killed tumour cells are gradually replaced by fibrosis and scar tissue. The treated tissue shrinks over the period of a few months. For instance, a coagulated 5 cm zone may be shrunk to as small as 2 cm.

The procedure as depicted in Figure 1 is called monopolar mode of RFA. It is characterised by the ground pad being pasted on patient's skin. RF current flows back and forth between the electrode and the ground pad. Despite its advantageous simplicity, the monopolar mode of RFA procedure has some drawbacks: the skin may be burned along the edges of the ground pad, the heat is concentric immediately adjacent to the electrode, leading to rapid charring and power shutoff. To overcome these drawbacks, the bipolar mode of RFA has been developed, in which a second parallel electrode is used instead of the ground pad. Besides, many other techniques for improvement have been developed, such as the expendable electrode, the cooled electrode (cooling water is circulated inside electrode), the wet electrode (saline is infused from inside of electrode to surrounding issue) and the saline-enhanced RFA (saline is directly injected into the tissue near the electrode tip). A detailed description of these RFA techniques may be found elsewhere (Mulier et al., 2005).

In principle, RFA may involve multidisciplinary sciences, e.g., the electricity, the thermal transfer and fluid mechanics (blood flow in vessels and seepage of saline through tissue). The variables identified to have significant impact on RF heating include electrical conductivity of the tumour and surrounding tissue, thermal conductivity of tissue, tissue perfusion and RF generator output. The

response of liver and tumour tissues to the thermal effect depends upon several factors including tissue material properties, ablation duration, temperature- or power-control mode of ablation, tumour location and the electrode geometry.

Since hepatic RFA technique is relatively new, the high local recurrence rates might be due to inadequate electrode designs, placements or overheating of the tissue in close proximity to the electrode. These factors may contribute to incomplete destruction of tumour cells. Therefore, computer modelling is unquestionably useful for optimising the RFA procedures in clinical practice.

Although computer modelling, in most cases, is based on numerical methods such as finite element methods and finite difference methods, analytical solutions may give fundamental insight on the very mathematical and physical nature of RFA. We have found in the literature three analytical solutions: the temperature distribution due to a cylindrical electrode of finite length in an infinite medium (Cheng et al., 1998), a straight segment of electrode embedded in a box of finite size (Johnson and Saidel, 2002) and a point source of electric current in an infinite medium (Jiang et al., 2007). Because of difficulty to find analytical solutions for real RFA problems, much more efforts have been devoted to numerical solutions. A 3D finite element analysis for monopolar RFA with the expendable electrode has been reported (Tungjitkusolmun et al., 2002). The study was extended to bipolar RFA (Haemmerich et al., 2001) which was further extended to take into account blood vessels close to electrodes with assumed fully developed flow velocity (Haemmerich et al., 2003a). Cooling effect in RFA with cooled electrodes was studied with an asymmetrical model (Haemmerich et al., 2003b). An Arrhenius tissue damage model, which considers the temperature history, was used to calculate thermal dose within the tissue to compare with the RFA lesion boundaries determined by the 50°C isotherm. It has been found that the 50°C isotherm predicted the lesion with acceptable accuracy (Haemmerich et al., 2003c). In a study where the temperature controlled RFA was simulated, the authors implemented a control algorithm for a proportional-integral (PI) controller, a commonly used controller type, in a C++ program to change the applied voltage between the time steps. The controller ran together with ABAQUS (Haemmerich and Webster, 2005). A finite element analysis on RFA using a temperature-dependent conductivity of a sodium chloride solution has been performed. It is assumed that the temperature-dependent behaviour of liver tissue is similar to that of an equivalent sodium chloride solution. A slightly non-linear behaviour due to two way-coupling of electricity and thermal fields has been observed (Chang, 2003). With finite element modelling, effects on RFA by changing the electrical conductivity, the thermal conductivity, the perfusion and the generator power has been studied (Liu et al, 2005). Three-dimensional blood flow through a real porcine arterial model reconstructed from MRI images has been computed. Navier-Stokes equations together with the energy equation within the

artery were then solved with the FEM. Instead of the resistive heating, Gaussian-distributed RF heat source was placed nearby the artery (Hariharan et al., 2007). A first attention has been given to the simulation of the saline infiltration effect in RFA in which the saline infusion in tissue was not computed but its consequence on the change in the electrical conductivity of tissue was directly assumed (Berjano et al., 2006). Thereafter, in a more rigorous study, Darcy's flow in porous medium was used to model the saline infiltration in tissue. The computed velocity of the saline infiltration is then introduced in the heat convective term in the energy equation (Barauskasa et al., 2008).

The above cited studies demonstrate a clear progress in mathematical modelling of RFA. More and more factors influencing RFA have been taken into account at the price of increasing complexity of the analysis. Besides, these studies relied on finite element codes of general purpose such as PATRAN, ABAQUS, FEMLAB or COMSOL. To use these codes, long-term special training is necessary even for people of good background in physics or mathematics or engineering. The use of these finite element codes of general purpose would become undoubtedly more challenging for RFA clinicians. On the other hand, they do need a tool to optimise the RFA process and to predict clinical results.

Johnson and Saidel followed this line and proposed a semi-analytical model (Johnson and Saidel, 2002). Although their model worked very fast, from a few seconds to a few minutes using a PC, it is limited to the monopolar RFA and to very limited geometry of tissue and of electrodes. The limitations of Johnson's model may be easily overcome with FEM. Of course, as compared with his semi-analytical model, FEM needs more computational time and resources. But, with rapid progress in computer technology, it is now possible to obtain finite element solutions of realistic RFA problem within a few minutes or, in a very near future, within a few seconds. It is in this perspective view that we propose in this study a specific finite element formulation for fast analysis of RFA.

2 Formulation of 3D FEM for RFA

2.1 Governing equations

RFA operates between 460–550 kHz. At these frequencies, the wavelength is about 600 metres. The inter-polar distance is in order of one meter in case of monopolar RFA or a few centimetres in case of bipolar RFA. The wavelength of RF current is thus two to four orders of magnitude longer than inter-polar distance. Therefore, the ablation probe dissipates the majority of its energy through electrical conduction and not capacitive coupling. We may thus solve the electric potential by using Laplace's equation in assuming a quasi-static electrical conduction model.

$$\frac{\partial^2 V}{\partial x^2} + \frac{\partial^2 V}{\partial y^2} + \frac{\partial^2 V}{\partial z^2} = 0 \quad (1)$$

where V is the electric potential (volts). It was assumed that tissues may be considered as a homogeneous medium with constant electric and thermal conductivities.

Heat transfer in tissue is governed by the so-called bioheat equation

$$\rho c \frac{\partial T}{\partial t} = k \left(\frac{\partial^2 T}{\partial x^2} + \frac{\partial^2 T}{\partial y^2} + \frac{\partial^2 T}{\partial z^2} \right) + \mathbf{j} \cdot \mathbf{E} - \rho_b C_b \omega (T - T_{amb}) + Q_m \quad (2)$$

where ρ is the density (kg/m³), c is the heat capacity (J/kg-K), k denotes constant heat conduction coefficients (W/K-m). ρ_b is the density of blood, C_b is the heat capacity of blood, ω is the blood perfusion coefficient, T_{amb} is the ambient temperature and Q_m is the metabolic heat source term. In equation (2), the most important heat source is due to the scalar product, $\mathbf{j} \cdot \mathbf{E}$. It represents the Joule heating in which \mathbf{j} denotes the current density vector (A/m²) and \mathbf{E} the electricity field density vector (V/m). In this study, the Joule heat source is taken into account while the blood perfusion and the metabolic heat source term are neglected. In this case, the bioheat equation (2) is reduced to that one may encounter in thermal-electric analysis:

$$\rho c \frac{\partial T}{\partial t} = \left(k_x \frac{\partial^2 T}{\partial x^2} + k_y \frac{\partial^2 T}{\partial y^2} + k_z \frac{\partial^2 T}{\partial z^2} \right) + \mathbf{j} \cdot \mathbf{E} \quad (3)$$

The electricity field density \mathbf{E} is equal to the negative gradient of the potential V :

$$\mathbf{E} = -\nabla V = -\left(\frac{\partial V}{\partial x} + \frac{\partial V}{\partial y} + \frac{\partial V}{\partial z} \right) \quad (4)$$

The current density \mathbf{j} is related to the electric field density by

$$\mathbf{j} = \frac{\mathbf{E}}{\sigma} \quad (5)$$

in which σ is the electric resistivity (Ω/m).

The source term due to Joule heating may be computed as

$$q = \mathbf{j} \cdot \mathbf{E} = \frac{1}{\sigma} \left[\left(\frac{\partial V}{\partial x} \right)^2 + \left(\frac{\partial V}{\partial y} \right)^2 + \left(\frac{\partial V}{\partial z} \right)^2 \right] \quad (6)$$

As the electric potential V appears in the heat source term of the thermal equation (3), the temperature T is influenced by the electric potential. However, the electric potential is not influenced by the temperature as no temperature appears in equation (1). This one-way coupling is a consequence of constant electric parameters. If electric parameters vary in function of temperature, the temperature change will lead to change in the electric parameters which results in the electric potential change. Equation (1) and equation (3) will be then fully coupled. This case has been discussed in (Chang, 2003).

2.2 Weak forms of governing equations

Finite element methods are based on weak forms of partial differential equations. The weak form of equation (1) defined on the domain of an element, Ω_e , may be written as

$$\int_{\Omega_e} \phi \left[\frac{\partial^2 V}{\partial x^2} + \frac{\partial^2 V}{\partial y^2} + \frac{\partial^2 V}{\partial z^2} \right] d\Omega = 0 \quad (7)$$

in which ϕ is an arbitrary test function. Similarly, the weak form of equation (3) defined on Ω_e may be written as

$$\int_{\Omega_e} \phi \left[-\rho c \frac{\partial T}{\partial t} + k \left(\frac{\partial^2 T}{\partial x^2} + \frac{\partial^2 T}{\partial y^2} + \frac{\partial^2 T}{\partial z^2} \right) + q \right] d\Omega_e = 0 \quad (8)$$

In order to reduce the order of differentiation on the field variables V and T , the above two weak forms of partial differential equations may be transformed with the following theorem of divergence:

$$\int_{\Omega} (\nabla F) \cdot G d\Omega = - \int_{\Omega} (\nabla G) \cdot F d\Omega + \int_{\Gamma} (\bar{n} \cdot F) \cdot G d\Gamma \quad (9)$$

in which F and G are two arbitrary differentiable functions of first order, Ω and Γ are domain and its boundary respectively, \bar{n} is the outward normal direction of boundary Γ .

The application of the theorem of divergence to equation (7) leads to:

$$- \int_{\Omega_e} \left[\frac{\partial \phi}{\partial x} \frac{\partial V}{\partial x} + \frac{\partial \phi}{\partial y} \frac{\partial V}{\partial y} + \frac{\partial \phi}{\partial z} \frac{\partial V}{\partial z} \right] d\Omega + \int_{\Gamma} \phi \frac{\partial V}{\partial n} d\Gamma = 0 \quad (10)$$

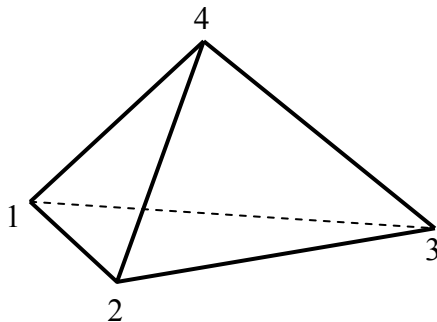
Similarly, applying the theorem of divergence to equation (8), one obtained:

$$\begin{aligned} & - \int_{\Omega_e} k \left(\frac{\partial \phi}{\partial x} \frac{\partial T}{\partial x} + \frac{\partial \phi}{\partial y} \frac{\partial T}{\partial y} + \frac{\partial \phi}{\partial z} \frac{\partial T}{\partial z} \right) d\Omega_e \\ & + \int_{\Gamma_e} \phi \frac{\partial T}{\partial n} d\Gamma_e + \int_{\Omega_e} \phi q d\Omega_e - \int_{\Omega_e} \left(\rho c \frac{\partial T}{\partial t} \right) d\Omega_e = 0 \end{aligned} \quad (11)$$

2.3 Stiffness matrices of finite elements

A first-order tetrahedral element of four nodes, as depicted in Figure 2, is to be developed hereafter.

Figure 2 Tetrahedral element



The finite element method approximates equations (10) and (11) by substitution of field variables, V and T , with help of interpolation functions within element. For the tetrahedral element of four nodes, the field value at any point inside the element may be interpolated with field values at four element vertices. This may be expressed as the following equations in which V_i and T_i ($i = 1, 2, 3, 4$) are potential and temperature values at element vertices, ϕ_1, ϕ_2, ϕ_3 and ϕ_4 are interpolation functions.

$$V = \phi \cdot V = \sum_{i=1}^4 \phi_i V_i \quad (12)$$

$$T = \phi \cdot T = \sum_{i=1}^4 \phi_i T_i \quad (13)$$

$$\phi = [\xi \quad \eta \quad \zeta \quad 1 - \xi - \eta - \zeta] \quad (14)$$

ξ, η and ζ are called intrinsic coordinates. Their values vary between 0 and 1.

In equations (12) and (13), we have used deliberately the same symbol, ϕ , as used to denote the test function in the weak forms, equations (10) and (11). This is because we actually use the same functions for both the interpolation and the test functions. Finite element formulations using the same functions for the interpolation and the test functions are called the Galerkin method. It leads to a symmetrical stiffness matrix.

Substituting V, T and in equations (10) and (11) with their expressions given in equations (12), (13) and (14), we obtain following two approximate (due to the interpolation) piecewise weak forms in which subscribe indices $i = 1..4, j = 1..4, k = 1..3$ and the Einstein summation convention is applied.

$$- \int_{\Omega_e} \frac{\partial \phi_i}{\partial x_k} \frac{\partial \phi_j}{\partial x_k} V_j d\Omega_e + \int_{\Gamma} \phi_i \phi_j \frac{\partial V_j}{\partial n} d\Gamma = 0 \quad (15)$$

$$\int_{\Omega_e} \rho c \phi_i \phi_j \frac{\partial T_j}{\partial t} d\Omega_e + \int_{\Omega_e} k \frac{\partial \phi_i}{\partial x_k} \cdot \frac{\partial \phi_j}{\partial x_k} T_j d\Omega_e - \int_{\Gamma_e} \phi_i \phi_j \frac{\partial T_j}{\partial n} d\Gamma_e - \int_{\Omega_e} \phi_i q d\Omega_e = 0 \quad (16)$$

In equations (15) and (16), integrals

$$K_v = \int_{\Omega_e} \frac{\partial \phi_i}{\partial x_k} \frac{\partial \phi_j}{\partial x_k} d\Omega_e \quad (17)$$

and

$$K_T = \int_{\Omega_e} k \frac{\partial \phi_i}{\partial x_k} \frac{\partial \phi_j}{\partial x_k} d\Omega_e \quad (18)$$

will lead to two 4×4 matrices which are called stiffness matrices.

2.4 Analytical evaluation of stiffness matrices

Stiffness matrices are usually evaluated with Gauss quadrature. However, for the purpose of computational efficiency and accuracy, analytical expressions of stiffness matrices are to be deduced in this study. This is possible because the integral functions in equations (17) and (18) are constant. To prove this, it is sufficient to show that derivatives of the interpolation function with reference to coordinates (letting $x = x_1, y = x_2, z = x_3$) are constant, i.e.,

$$\frac{\partial \phi_i}{\partial x_k} = \text{constant} \quad (19)$$

Notice that the interpolation functions are defined in function of local coordinate ξ, η and ζ in equation (14). Derivatives of interpolation function with reference to local coordinate, ξ, η and ζ , are related to that with reference to global coordinates, x, y and z by the following relationship:

$$\begin{Bmatrix} \frac{\partial \phi_i}{\partial \xi} \\ \frac{\partial \phi_i}{\partial \eta} \\ \frac{\partial \phi_i}{\partial \zeta} \end{Bmatrix} = \begin{bmatrix} \frac{\partial x}{\partial \xi} & \frac{\partial y}{\partial \xi} & \frac{\partial z}{\partial \xi} \\ \frac{\partial x}{\partial \eta} & \frac{\partial y}{\partial \eta} & \frac{\partial z}{\partial \eta} \\ \frac{\partial x}{\partial \zeta} & \frac{\partial y}{\partial \zeta} & \frac{\partial z}{\partial \zeta} \end{bmatrix} \begin{Bmatrix} \frac{\partial \phi_i}{\partial x} \\ \frac{\partial \phi_i}{\partial y} \\ \frac{\partial \phi_i}{\partial z} \end{Bmatrix} = \mathbf{J}^T \begin{Bmatrix} \frac{\partial \phi_i}{\partial x} \\ \frac{\partial \phi_i}{\partial y} \\ \frac{\partial \phi_i}{\partial z} \end{Bmatrix} \quad (20)$$

in which \mathbf{J} is the Jacobian matrix defined as:

$$\mathbf{J} = \begin{bmatrix} \frac{\partial x}{\partial \xi} & \frac{\partial x}{\partial \eta} & \frac{\partial x}{\partial \zeta} \\ \frac{\partial y}{\partial \xi} & \frac{\partial y}{\partial \eta} & \frac{\partial y}{\partial \zeta} \\ \frac{\partial z}{\partial \xi} & \frac{\partial z}{\partial \eta} & \frac{\partial z}{\partial \zeta} \end{bmatrix} \quad (21)$$

By using the isoparametric element (interpolation function = shape function), we assume that coordinates at any point inside element may be interpolated in the same way as the interpolation of the field variables, i.e.,

$$\begin{Bmatrix} x \\ y \\ z \end{Bmatrix}^T = [\phi_1 \quad \phi_2 \quad \phi_3 \quad \phi_4] \begin{Bmatrix} x_1 & y_1 & z_1 \\ x_2 & y_2 & z_2 \\ x_3 & y_3 & z_3 \\ x_4 & y_4 & z_4 \end{Bmatrix} \quad (22)$$

Substitution of equation (22) into equation (21) leads to

$$\mathbf{J} = \begin{bmatrix} x_1 & x_2 & x_3 & x_4 \\ y_1 & y_2 & y_3 & y_4 \\ z_1 & z_2 & z_3 & z_4 \end{bmatrix} \begin{bmatrix} \frac{\partial \phi_1}{\partial \xi} & \frac{\partial \phi_1}{\partial \eta} & \frac{\partial \phi_1}{\partial \zeta} \\ \frac{\partial \phi_2}{\partial \xi} & \frac{\partial \phi_2}{\partial \eta} & \frac{\partial \phi_2}{\partial \zeta} \\ \frac{\partial \phi_3}{\partial \xi} & \frac{\partial \phi_3}{\partial \eta} & \frac{\partial \phi_3}{\partial \zeta} \\ \frac{\partial \phi_4}{\partial \xi} & \frac{\partial \phi_4}{\partial \eta} & \frac{\partial \phi_4}{\partial \zeta} \end{bmatrix} \quad (23)$$

$$= \begin{bmatrix} x_1 - x_4 & x_2 - x_4 & x_3 - x_4 \\ y_1 - y_4 & y_2 - y_4 & y_3 - y_4 \\ z_1 - z_4 & z_2 - z_4 & z_3 - z_4 \end{bmatrix}$$

The Jacobian matrix is thus constant as its elements are only formed with nodal coordinates of the finite element mesh which are given constant data. Solving equation (20) for derivatives of interpolation functions with reference to global coordinates, we obtain

$$\begin{Bmatrix} \frac{\partial \phi_i}{\partial x} \\ \frac{\partial \phi_i}{\partial y} \\ \frac{\partial \phi_i}{\partial z} \end{Bmatrix} = [\mathbf{J}^T]^{-1} \begin{Bmatrix} \frac{\partial \phi_i}{\partial \xi} \\ \frac{\partial \phi_i}{\partial \eta} \\ \frac{\partial \phi_i}{\partial \zeta} \end{Bmatrix} \quad (24)$$

where $[\mathbf{J}^T]^{-1}$ denotes the inverse of the transpose of the Jacobian matrix. As the Jacobian matrix is constant, the inverse matrix, $[\mathbf{J}^T]^{-1}$, is obviously constant. Hence, derivatives of interpolation functions with reference to global coordinates given in equation (22) are constant. Consequently, we can move those derivatives out of integral operator in equations (17):

$$\mathbf{K}_v = \frac{\partial \phi_i}{\partial x_k} \frac{\partial \phi_j}{\partial x_k} \int_{\Omega_e} d\Omega_e = \frac{\partial \phi_i}{\partial x_k} \frac{\partial \phi_j}{\partial x_k} \text{Vol} \quad (25)$$

in which Vol denotes the element volume. The volume of a tetrahedral element is equal to the sixth of Jacobian:

$$\text{Vol} = \frac{|\mathbf{J}|}{6} \quad (26)$$

Similarly, the stiffness matrix in equation (18) is equal to

$$\mathbf{K}_T = k \frac{\partial \phi_i}{\partial x_k} \frac{\partial \phi_j}{\partial x_k} \int_{\Omega_e} d\Omega_e = k \frac{\partial \phi_i}{\partial x_k} \frac{\partial \phi_j}{\partial x_k} \text{Vol} \quad (27)$$

To evaluate derivatives of interpolation functions with reference to global coordinates as given in equation (24), we need to evaluate the inverse matrix, $[\mathbf{J}^T]^{-1}$ and derivatives of interpolation functions with reference to local coordinates. The latter is straightforward as interpolation functions are defined in local coordinates, see equation (14). The former may be evaluated by using the standard mathematical definition of the inverse matrix:

$$\begin{aligned} [\mathbf{J}^T]^{-1} &= \frac{1}{|\mathbf{J}^T|} \begin{bmatrix} X_{14} & X_{24} & X_{34} \\ Y_{14} & Y_{24} & Y_{34} \\ Z_{14} & Z_{24} & Z_{34} \end{bmatrix} \\ &= \frac{1}{|\mathbf{J}|} \begin{bmatrix} X_{14} & X_{24} & X_{34} \\ Y_{14} & Y_{24} & Y_{34} \\ Z_{14} & Z_{24} & Z_{34} \end{bmatrix} \end{aligned} \quad (28)$$

in which X_{14} denotes the cofactor of element (x_1-x_4) in \mathbf{J} and so on. We have substituted the determinant, $|\mathbf{J}^T|$, with Jacobian, $|\mathbf{J}|$, as they are equal. Cofactors may be computed with the following relationships.

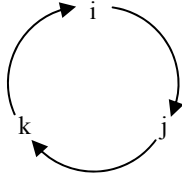
$$X_{i4} = \begin{vmatrix} y_j - y_4 & y_k - y_4 \\ z_j - z_4 & z_k - z_4 \end{vmatrix} \quad (29)$$

$$Y_{i4} = \begin{vmatrix} z_j - z_4 & z_k - z_4 \\ x_j - x_4 & x_k - x_4 \end{vmatrix} \quad (30)$$

$$Z_{i4} = \begin{vmatrix} x_j - x_4 & x_k - x_4 \\ y_j - y_4 & y_k - y_4 \end{vmatrix} \quad (31)$$

The mutation of indices follows the order as depicted in Figure 3. For instance, if $i = 1$, then $j = 2$ and $k = 3$; if $i = 2$, then $j = 3$ and $k = 1$; if $i = 3$, then $j = 1$ and $k = 2$ and so on. Substituting the above inverse matrix into equation (24), we obtained, in a matrix form, derivatives of interpolation functions with reference to global coordinates as followings:

Figure 3 Mutation of element indices



$$\begin{aligned} &\begin{bmatrix} \frac{\partial \phi_1}{\partial x} & \frac{\partial \phi_2}{\partial x} & \frac{\partial \phi_3}{\partial x} & \frac{\partial \phi_4}{\partial x} \\ \frac{\partial \phi_1}{\partial y} & \frac{\partial \phi_2}{\partial y} & \frac{\partial \phi_3}{\partial y} & \frac{\partial \phi_4}{\partial y} \\ \frac{\partial \phi_1}{\partial z} & \frac{\partial \phi_2}{\partial z} & \frac{\partial \phi_3}{\partial z} & \frac{\partial \phi_4}{\partial z} \end{bmatrix} \\ &= \frac{1}{|\mathbf{J}|} \begin{bmatrix} X_{14} & X_{24} & X_{34} & -X_{14} - X_{24} - X_{34} \\ Y_{14} & Y_{24} & Y_{34} & -Y_{14} - Y_{24} - Y_{34} \\ Z_{14} & Z_{24} & Z_{34} & -Z_{14} - Z_{24} - Z_{34} \end{bmatrix} \end{aligned} \quad (32)$$

2.5 Analytical evaluation of the heat source term due to Joule effect

When only Joule heating is taken into account in the bioheat equation, the heat source term in the weak form, equation (16), may be evaluated analytically within a tetrahedral element.

$$I_{\text{Joule}} = \int_{\Omega_e} \phi_i q d\Omega_e = \int_{\Omega_e} \phi_i (\mathbf{j} \cdot \mathbf{E}) d\Omega_e \quad (33)$$

In a first-order tetrahedral element, the potential is in linear function of coordinates and the potential gradient is constant. Consequently, according to equations (5) and (6), both the current density \mathbf{j} and the electricity field density \mathbf{E} are constant. They may be then moved out the integral operator.

$$I_{\text{Joule}} = (\mathbf{j} \cdot \mathbf{E}) \int_{\Omega_e} \phi_i d\Omega_e \quad (34)$$

The remaining integral can be evaluated analytically as below:

$$\begin{aligned} \int_{\Omega_e} \phi_i d\Omega_e &= \int_0^1 \int_0^{1-\zeta} \int_0^{1-\eta-\zeta} \phi_i |\mathbf{J}| d\xi d\eta d\zeta \\ &= |\mathbf{J}| \int_0^1 \int_0^{1-\zeta} \int_0^{1-\eta-\zeta} \phi_i d\xi d\eta d\zeta \end{aligned} \quad (35)$$

It has been found in this study the following extreme simple value of the integral in the above equation:

$$\int_0^1 \int_0^{1-\zeta} \int_0^{1-\eta-\zeta} \phi_i d\xi d\eta d\zeta \equiv \frac{1}{24}, i = 1 \dots 4 \quad (36)$$

Hence, in combining this result together with equation (35), we have found the heat source term due to Joule effect in equation (33) equal to

$$I_{\text{Joule}} = (\mathbf{j} \cdot \mathbf{E}) \frac{1}{24} |\mathbf{J}| = \frac{\text{Vol}}{4} (\mathbf{j} \cdot \mathbf{E}) \quad (37)$$

Recall that the product, $\mathbf{j} \cdot \mathbf{E}$, has been given in equation (6).

2.6 Time matching

The temporary behaviour of RFA is dealt with the term containing the partial derivative of temperature with reference to time in the weak form equation (16), i.e., the term:

$$\int_{\Omega_e} \rho c \phi_i \phi_j \frac{\partial T_j}{\partial t} d\Omega_e = M_e \begin{Bmatrix} \frac{\partial T_1}{\partial t} \\ \frac{\partial T_2}{\partial t} \\ \frac{\partial T_3}{\partial t} \\ \frac{\partial T_4}{\partial t} \end{Bmatrix} \quad (38)$$

in which M_e is called the mass matrix defined as:

$$M_e = \rho c \int_{\Omega_e} \begin{Bmatrix} \phi_1 \\ \phi_2 \\ \phi_3 \\ \phi_4 \end{Bmatrix} \begin{bmatrix} \phi_1 & \phi_2 & \phi_3 & \phi_4 \end{bmatrix} d\Omega_e \quad (39)$$

The mass matrix may be evaluated in the same way as in equation (34):

$$M_e = \rho c \int_0^1 \int_0^{1-\zeta} \int_0^{1-\eta-\zeta} \begin{Bmatrix} \phi_1 \\ \phi_2 \\ \phi_3 \\ \phi_4 \end{Bmatrix} [\phi_1 \ \phi_2 \ \phi_3 \ \phi_4] |J| d\xi d\eta d\zeta \quad (40)$$

Substituting interpolation functions defined in equation (14) into (40) and evaluating all ten different integrals, we obtained

$$M_e = \frac{\rho \cdot c \cdot \text{Vol}}{20} \begin{bmatrix} 2 & 1 & 1 & 1 \\ 1 & 2 & 1 & 1 \\ 1 & 1 & 2 & 1 \\ 1 & 1 & 1 & 2 \end{bmatrix} \quad (41)$$

For some reasons unknown to the authors up to now, this mass matrix may result in negative temperature, although correct theoretically. Hence, it is not used in author's program. Instead, the following lumped mass is used which is obtained with the so called row-sum technique (Hughes, 1987) consisting in summing the elements in each row and lumping on the diagonal and vanishing the off-diagonal elements.

$$M_e = \frac{\rho \cdot c \cdot \text{Vol}}{20} \begin{bmatrix} 5 & 0 & 0 & 0 \\ 0 & 5 & 0 & 0 \\ 0 & 0 & 5 & 0 \\ 0 & 0 & 0 & 5 \end{bmatrix} \quad (42)$$

Time marching

Denoting time at n th step by t_n , time at $(n - 1)$ th step by t_{n-1} , time increment from t_{n-1} to t_n by Δt_n , we have

$$t_n = t_{n-1} + \Delta t_n \quad (43)$$

The time derivative of temperature at node i at n th time step may be approximated by the difference:

$$\frac{\partial T_i}{\partial t} \approx \frac{T_i^{n+1} - T_i^n}{\Delta t_n} = \frac{dT_i^n}{\Delta t_n} \quad (44)$$

in which superscripts of T denote time steps while subscripts of T stand for nodal numbers. Let us denote

$$F_e^n = -\oint_{\Gamma_e} \phi \frac{\partial T}{\partial n} d\Gamma_e - \int_{\Omega_e} \phi (\mathbf{j} \cdot \mathbf{E}) d\Omega_e \\ = -\int_{\Omega_e} \phi (\mathbf{j} \cdot \mathbf{E}) d\Omega_e = -\frac{\text{Vol}}{4} \mathbf{j} \cdot \mathbf{E} \quad (45)$$

in which the term, $\oint_{\Gamma_e} \phi \frac{\partial T}{\partial n} d\Gamma_e$, disappeared in the final expression because on the boundary Γ , the normal gradient of temperature, $\frac{\partial T}{\partial n}$, is generally prescribed to be zero and

on interfaces between elements, its resultant is zero. Equation (16) may be rewritten in matrix form as following in which the stiffness K_T has been given in equation (27).

$$M_e \begin{Bmatrix} \frac{\partial T_1}{\partial t} \\ \frac{\partial T_2}{\partial t} \\ \frac{\partial T_3}{\partial t} \\ \frac{\partial T_4}{\partial t} \end{Bmatrix} + K_T \begin{Bmatrix} T_1 \\ T_2 \\ T_3 \\ T_4 \end{Bmatrix} + F_e = 0 \quad (46)$$

Solving the above equation for time derivatives, we express time derivatives of temperature in function of temperature.

$$\begin{Bmatrix} \frac{\partial T_1}{\partial t} \\ \frac{\partial T_2}{\partial t} \\ \frac{\partial T_3}{\partial t} \\ \frac{\partial T_4}{\partial t} \end{Bmatrix} = -M_e^{-1} \left[K_T \begin{Bmatrix} T_1 \\ T_2 \\ T_3 \\ T_4 \end{Bmatrix} + F_e \right] = \mathbf{f} \begin{Bmatrix} T_1 \\ T_2 \\ T_3 \\ T_4 \end{Bmatrix} \quad (47)$$

Furthermore, on the other hand, time derivatives may be approximated with the following formula derived from the interpolation theory [Hughes, (1987), p.460].

$$\begin{Bmatrix} \frac{\partial T_1}{\partial t} \\ \frac{\partial T_2}{\partial t} \\ \frac{\partial T_3}{\partial t} \\ \frac{\partial T_4}{\partial t} \end{Bmatrix} = \theta \cdot \mathbf{f} \begin{Bmatrix} T_1^{n+1} \\ T_2^{n+1} \\ T_3^{n+1} \\ T_4^{n+1} \end{Bmatrix} + (1-\theta) \cdot \mathbf{f} \begin{Bmatrix} T_1^n \\ T_2^n \\ T_3^n \\ T_4^n \end{Bmatrix} \quad (48)$$

in which θ is a parameter varying in the interval $[0, 1]$. In the present work, θ is equal to 0.5, which corresponds to Crank-Nicolson's method. Substituting time derivatives with time differentials as defined in equation (44) and combining equations (47) and (48), we obtain the following equation for the solution of temperature at $(n + 1)$ th time step with known values of temperature and of the source term at n th time step.

$$[M_e + \Delta t_n \theta \cdot K_T] \begin{Bmatrix} T_1^{n+1} \\ T_2^{n+1} \\ T_3^{n+1} \\ T_4^{n+1} \end{Bmatrix} \\ = [M_e - \Delta t_n (1-\theta) K_T] \begin{Bmatrix} T_1^n \\ T_2^n \\ T_3^n \\ T_4^n \end{Bmatrix} - \Delta t_n F_e^n \quad (49)$$

This is an implicit time matching scheme.

3 Test examples

Finite element formulas developed in foregoing sections have been implemented in C++. It will be added with a graphic user interface, an automatic mesh generator and a postprocessor. All will be extremely specialised for clinicians. The solver for the system of linear equations is based on the LU decomposition and the frontal method. The resulted program is named as RAFEM – Radiofrequency Ablation Finite Element Method. A free version of C++ compiler, Dev-C++ 5 Beta 9.2 (4.9.9.2) for Windows, is adopted. The following two examples are tested.

3.1 Static analysis

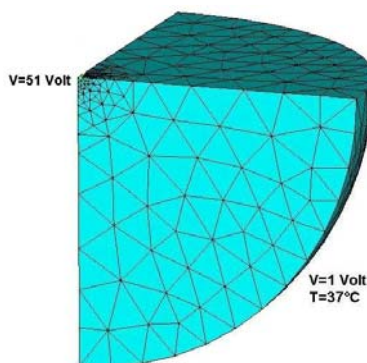
A source of current which has the potential of 51 volts is applied to the centre of a sphere. The sphere has radius of 1 metre. On its surface are applied the potential of 1 volt and the temperature of 37°C. Material data of the sphere as shown in Table 1 are the same as that of liver, taken from literatures (Tungjtkusolmun et al., 2002).

We need to determine the potential and the temperature fields in the sphere. Due to the symmetry, only an eighth of the sphere is analysed. The finite element mesh is shown in Figure 4, which is composed of 2,286 tetrahedral elements and of 595 nodes.

Table 1 Thermal and electrical properties of liver

Name	Symbol	Unity	Value
Density	ρ	kg/m ³	1,060
Specific heat	C	J/kg·K	3,600
Heat conductivity	k	W/m·K	0.512
Resistivity	σ	Ω ·m	3.003

Figure 4 Finite element mesh: due to the symmetry, only an 8th sphere needed to be discretised (see online version for colours)



Note: Boundary conditions defined at the centre and on the sphere surface.

Computational results of potential and temperature against sphere radius are compared in Table 2.

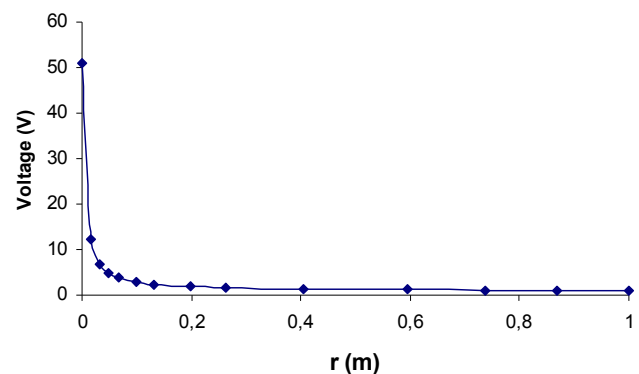
Table 2 Comparison of results of this work with ANSYS

Node	$x = r$ (mm)	ANSYS		This work	
		V (Volt)	T (°C)	V (Volt)	T (°C)
4	0.0	51.0	610.58	51.0	610.58
585	17	12.373	369.11	12.373	369.11
553	33	6.7431	213.00	6.7431	213.00
512	50	4.7968	155.52	4.7967	155.52
510	66	3.7932	125.14	3.7932	125.14
494	99	2.8096	94.720	2.8096	94.720
479	132	2.3240	79.434	2.3240	79.434
58	198	1.8071	63.019	1.8071	63.018
57	264	1.5697	55.408	1.5697	55.407
56	405	1.3346	47.837	1.3346	47.837

It can be seen that results given by RAFEM are almost identical to that by ANSYS. Only three numbers (in italics) are different in the fifth digit. This very slight difference may be explained by the fact that RAFEM uses the simple precision for real numbers (the type ‘float’ in C++) while ANSYS uses the double precision.

Curves of the potential and the temperature values against radius are drawn in Figures 5 and 6 respectively.

Figure 5 Voltage along radius (see online version for colours)



It can be observed that both potential and temperature have a sharp concentration around the sphere centre, i.e., when $r \rightarrow 0$. The temperature value of 610.58°C at the centre is actually an approximation by the finite element computation to the theoretical infinite value at that point. With polynomial functions as the interpolation function, finite elements can only give limited values.

Based on these results, we can conclude that the formulation and the implementation of tetrahedral elements as presented in previous sections are correct for the RFA static analysis. We need now to check the dynamic part, i.e., time matching.

3.2 Dynamic analysis

All real RFA problems are dynamic ones because real RFA procedures are limited in time, generally 12 to 30 minutes. Let us consider the sphere in the previous section as a dynamic problem and compute RFA procedure time up to

30 minutes. Temperature results along x-axis of this work are compared in Table 3 with that obtained with ANSYS. The two solutions are identical except at node 553 where there is a difference of 0.0016%. This is an excellent indication that RAFEM works correctly for dynamic RFA analysis. The static solution corresponds to the infinite time. In Figure 7 are drawn two curves of temperature: one corresponds to temperature at 30 minutes (dynamic solution), the other is the static solution which corresponds actually to the infinite time. It can be observed that heat transfer in liver material is quite slow: after 30 minutes of RFA procedure, high temperature zone is still confined nearby the sphere centre.

Table 3 Comparison of temperature of dynamic analysis

Node	$x = r$ (mm)	Temperature ($^{\circ}\text{C}$)	
		ANSYS	This work
4	0.0	396.51	396.51
585	17	177.87	177.87
553	33	63.122	63.123
512	50	42.055	42.055
510	66	37.970	37.970
494	99	37.076	37.076
479	132	37.021	37.021
58	198	37.005	37.005
57	264	37.001	37.001
56	405	37.000	37.000

Figure 6 Temperature along radius (see online version for colours)

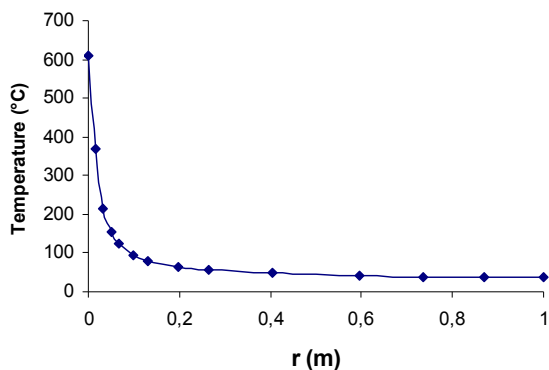
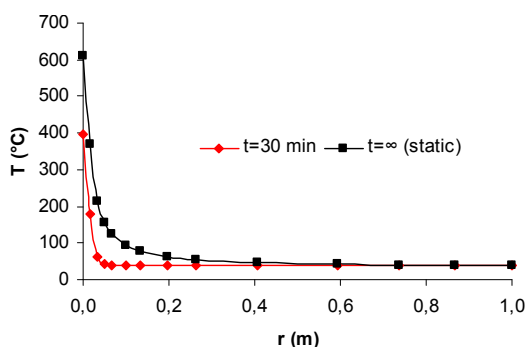


Figure 7 Comparison of temperature along radius of static and dynamic analysis (see online version for colours)



4 Discussion and conclusions

A finite element method specialised for RFA has been formulated in this study. By ‘specialised’, it means the simplicity and the robustness. These come from the fact that the method relies exclusively on linear tetrahedral element for field variables. This is feasible because RFA has an intrinsic feature: the thermal transfer in solid medium, which is relatively simple task with finite element methods. Besides, we are focused on a ‘simple’ objective: offer to clinicians a tool for qualitative prediction of RFA in routine practices. The robustness of the method relies on analytical integration of the stiffness matrix and Joule heat source term, as well as the frontal method for the solution of the system of linear equations. The LU decomposition is used so that in the time marching, only back substitutions are needed. To solve the two test examples, we used a Laptop of following characteristics: Intel Core 2 Duo CPU, T7700, 2.40 GHz, 3.5 GB of RAM. The CPU time for the dynamic RFA on the sphere (595 nodes and 2,286 elements) was about five seconds. Further reduction of CPU time is possible by using a solver more efficient than the classical frontal method, element-by-element time matching (Hughes, 1987), etc. As a future research, the formulation presented in this study may be extended to include equations necessary for describing the infusion and the perfusion of fluid in liver tissue and blood vessels.

Acknowledgements

This work was partially supported by MoSAIC and EU higher education project Asia-Link CfP 2006-EuropeAid/123738/C/ACT/Multi-Proposal No. 128-498/111.

References

- Barauskasa, R., Gulbinasb, A., Vanagasc, T. and Barauskasc, G. (2008) ‘Finite element modeling of cooled-tip probe radiofrequency ablation processes in liver tissue’, *Computers in Biology and Medicine*, Vol. 38, pp.694–708.
- Berjano, E., Burd, F., Navarro, A., Burd, J., Güemes, A., Aldana, O., Ros, P., Sousa, R., Lozano, R., Tejero, E. and Gregório, M. (2006) ‘Improved perfusion system for bipolar radiofrequency ablation of liver: preliminary findings from a computer modeling study’, *Physiol. Meas.*, Vol. 27, pp.N55–N66.
- Chang, I. (2003) ‘Finite element analysis of hepatic radiofrequency ablation probes using temperature-dependent electrical conductivity’, *BioMedical Engineering On Line*.
- Cheng, Y-C., Brown, R., Chung, Y., Duerk, J., Fujita, H., Lewin, J., Schuele, D. and Shvartsman, S. (1998) ‘Calculated RF electric field and temperature distributions in RF thermal ablation: comparison with gel experiments and liver imaging’, *Journal of Magnetic Resonance Imaging*, January–February, Vol. 8, No. 1, pp.70–76.
- Haemmerich, D. and Webster, J. (2005) ‘Automatic control of finite element models for temperature-controlled radiofrequency ablation’, *BioMedical Engineering On Line*, Vol. 4, p.42.

- Haemmerich, D., Chachati, L., Wright, A., Mahvi, D., Lee, F. and Webster, J. (2003a) 'Hepatic Radiofrequency ablation with internally cooled probes: effect of coolant temperature on lesion size', *IEEE Transactions on Biomedical Engineering*, Vol. 50, No. 4, April, pp.493–500.
- Haemmerich, D., Staelin, S., Tungjitkusolmun, S., Lee, F., Mahvi, D. and Webster, J. (2001) 'Hepatic bipolar radio-frequency ablation between separated multiprong electrodes', *IEEE Transactions on Biomedical Engineering*, Vol. 48, No. 10, October.
- Haemmerich, D., Webster, J. and Mahvi, D. (2003b) 'Thermal dose versus isotherm as lesion boundary estimator for cardiac and hepatic radio-frequency ablation', *Proceedings of the 25th Annual International Conference of the IEEE EMBS*, Cancun, Mexico, 17–21 September 2003.
- Haemmerich, D., Wright, A., Mahvi, D., Webster, J. and Lee, F. (2003c) 'Hepatic bipolar radiofrequency ablation creates coagulation zones close to blood vessels: a finite element study', *Medical & Biological Engineering & Computing*, Vol. 41, pp.317–323.
- Hariharan, P., Chang, I., Myers, M. and Banerjee, R. (2007) 'Radio-frequency ablation in a realistic reconstructed hepatic tissue', *Journal of Biomechanical Engineering*, June, Vol. 129, pp.354–364.
- Hughes, T. (1987) *The Finite Element Method, Linear Static and Dynamic Finite Element*, Prentice-Hall, Inc.
- Jiang, Y.S., Wang, C. Rambo, M.C.D., Bortolaia, L.A. and Valdiero, A.C. (2007) 'Analytical solution of temperature distribution in radiofrequency ablation due to a point source of electrical current', *Proceedings of 6th Brazilian Conference on Dynamics, Control and Their Applications*, 21–25 May 2007, UNESP, SP, Brazil.
- Johnson, P.C. and Saidel, G.M., (2002) 'Thermal model for fast simulation during magnetic resonance imaging guidance of radio frequency tumor ablation', *Annals of Biomedical Engineering*, Vol. 30, pp.1152–1161.
- Liu, Z., Lobo, S., Humphries, S., Horkan, C., Solazzo, S.A., Hines-Peralta, A., Lenkinski, R. and Goldberg, S. (2005) 'Radiofrequency tumor ablation: insight into improved efficacy using computer modeling', *American Journal of Roentgenology*, p.184, April.
- Mulier, S., Miao, Y., Mulier, P., Dupas, B., Pereira, P., de Baere, T., Lencioni, R., Leveillee, R., Marchal, G., Michel, L. and Ni, Y. (2005) 'Electrodes and multiple electrode systems for radiofrequency ablation: a proposal for updated terminology', *Eur Radiol*, Vol. 15, No. 4, pp.798–808 (Published online: 12 February 2005).
- Ni, Y., Mulier, S., Miao, Y., Michel, L. and Marchal, G. (2005) 'A review of the general aspects of radio frequency ablation', *Abdom Imaging*, Vol. 30, pp.381–400.
- Tungjitkusolmun, S., Staelin, S., Haemmerich, D., Tsai, J., Cao, H., Webster, J., Lee, F., Mahvi, D. and Vorperian, V. (2002) 'Three-dimensional finite-element analyses for radio-frequency hepatic tumor ablation', *IEEE Trans. Biomed. Eng.*, Vol. 49, pp.3–9.

Current address of Stefaan Mulier :

Stefaan Mulier, MD

Philipslaan 66

3000 Leuven

Belgium

+32 16 35 67 86

+32 498 78 73 57

stefaan.mulier@skynet.be

<http://drmulier.com/research.html>